Numerical Analysis of a Free Falling Wedge into Calm Water

João Maria Muralha
joao.muralha@tecnico.ulisboa.pt

Instituto Superior Técnico, Universidade de Lisboa, Portugal

November 2017

Abstract
This work presents a validation exercise of a mathematical model for the impact of a bidimensional wedge with 25° deadrise angle based on the experimental results of Lewis et al. (2010). The mathematical model assumes incompressible fluids, bi-dimensional flow and does not include surface tension effects and friction in the wedge surface, the fluid is a mixture of water and air with properties defined using the Volume of Fluid method (VOF). Prior to the validation process, convergence studies and investigation on the influence of the temporal derivative approximations, domain dimensions and grid types were performed.

The existence of a time delay between the numerical and experimental results for both pressure and acceleration was detected. Nevertheless, the maximum pressure values for each sensor are in close agreement with the experimental results. The same happened for pressure measured at relative time instances and the time difference between peak pressures in each sensor. Regarding the acceleration values, significant differences between the numerical and experimental results were detected.
Keywords: Water entry impact; Symmetric 2D wedge; Volume of fluid; Verification; Validation

1. Introduction

Impact loads during water entry of solid bodies have been the topic of many theoretical and experimental studies since the pioneering analytical works by von Karman (1929) and Wagner (1932).

This topic is of interest for both the industrial and academic communities, as it is decisive for the safety assessment of several applications, as water landing of aircrafts (Ellis, 2015), ship slamming (Reddy et al., 2002), wave impact in floating bodies (Sasson et al., 2016), and free fall lifeboats (Kamath et al., 2016).

Experimental studies of full scale or scaled models can still be considered the most reliable method for the assessment of the complex slamming loads that are involved in these applications. However, they are prohibitively costly and time consuming, in addition to the difficulties related to generalizing the results of specific experimental set-ups to wider universal usage. Recent years have witnessed the fast development of computer technology and numerical analysis, and computational fluid dynamics (CFD) has been increasingly applied in various areas as aerospace engineering, and as an important analysis and design tool in the ship industry (Qian et al., 2006). Nowadays, if properly validated by comparison with experimental results, computational methods can lead to efficient techniques of evaluating different cost effective options available at the design stage, since they offer the significant advantage of providing detailed insight into impact phenomena.

This work follows up on research work carried out in MARIN (Maritime Research Institute Netherlands) by Maximiano (2016) aiming at comparing CFD simulation results with experimental data following a comprehensive verifications and validation procedure (V&V).

Current applications of CFD use in.house, commercial or open source codes. As a contribution to increase knowledge and gain confidence in the use of the CFD solver ReFRESCO (`www.refresco.org`) for water impact loads applications, in this work a fundamental case of a free falling 25° deadrise angle 2D wedge into calm water is simulated and compared with experimental results obtained at the Southampton University (Lewis et al., 2010). To accomplish this main objective several tasks were performed:

- Analysis of the convergence properties of the numerical solution;
- Choice of the time derivative approximation;
- Influence of the domain size;
- Influence of the grid type in the numerical simulations.

2. Problem definition

Independently of the shape or entry velocity, the water entry of a free falling wedge can be divided in four stage (Wang et al., 2015): slamming; transition; collapse; and post-closure.

2.1. Mathematical model

For the development of the mathematical model presented in this work, only the first two stages are addressed, as only 100ms were simulated. Regarding the flow characteristics in these phases, the following assumptions were considered:

- Both water and air are considered incompressible;
- Water tension forces are considered negligible;
- The flow was considered laminar;
- The viscous forces on the wedge walls were not considered.

Furthermore the air volume fraction, α, transport equation introduced by the Volume of Fluid (VOF) method (Hirt and Nichols, 1981) in addition to the Navier-Stokes (NS) equations were used to model the flow. The movement of the wedge was simulated by displacing the wedge downwards, based on the results obtained by Maximiano (2016).

2.2. Domain dimensions, boundary and initial conditions

The simulation domain and boundary conditions are presented in Figure 1 and its dimensions in Table 1. A slip boundary condition was applied in the wedge surface and on the right side, a symmetry plane was considered in the left side. On the top and bottom, a pressure and hydrostatic pressure boundary conditions were applied. As ReFRESCO is a three-dimensional, code the simplification to bi-dimensional flow is done considering a mesh with a single cell with 0.1m in the out-of-plane direction and imposing symmetry boundary conditions to the limiting planes. Under this hypothesis, the wedge mass is proportionally reduced to 2.272kg. As shown in Figure 1, the wedge is initially considered to be at the water level with a downward velocity of 3.58m/s. The water and air were considered stationary at the initial time.

Table 1: Domain and wedge dimensions

Height			Width	h	b
AH/h	WD/h	H/h	W/b	[mm]	[mm]
5	10	15	5	210	450

2.3. Numerical solution

A numerical solution for the mathematical model was obtained using ReFRESCO. This code discretizes the equations using a finite-volume approach with cell-centred variables. A pressure-correction equation based on the SIMPLE algorithm is used to ensure mass conservation. Time integration can be performed implicitly using first or second order schemes. At each implicit time step, the non-linear system for velocity and pressure is linearized with Picard's method and a segregated approach is used (MARIN, 2017).

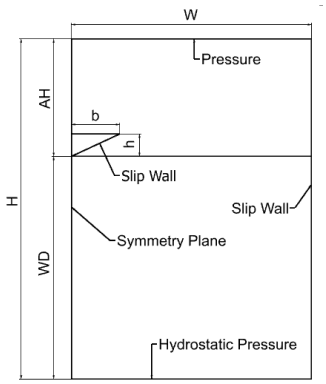

Figure 1: Scheme of the simulation domain

The wedge movement is considered to occur only in the vertical direction and it is simulated using a moving grid technique, as in the work of Maximiano (2016). In this approach the α and NS equations are solved in an Earth fixed reference frame, with the grid velocity applied in the convective velocity. It is important to point out that this technique does not allow the assessment of wall proximity effects, for the domain bottom. The velocity is calculated during the simulation (Reddy et al., 2002; Maximiano, 2016).

An investigation on the effect of the time derivative approximation was performed. The convective term in the momentum and free surface equations are discretized using the QUICK scheme and the Fromm scheme with a Total Variance Diminishing (TVD) Flux Limiter, respectively. The gradients were calculated based on the Gauss theorem.

In the present work both structured, generated using the tools described by Eça (2003), and unstructured, generated using Hexpress, grids sets were used (Tables 2 and 3). These grids defined six areas coincident with the locations of the pressure sensors in the experimental set-up, where ReFRESCO force monitors were used (Figure 2). The grids topologies are illustrated in Figure 3.

The convergence criterion was a normalized residual in the L2 norm less than 10^{-5}, in the structure grids this criterion was 5×10^{-6}.

Table 2: Typical grid size and number of time steps for the structured grids set

Grid	Number of cells in the wedge	$\frac{h_i}{h_1}$	Δt [s]					
			1st order in time			2nd order in time		
			t_1	t_2	t_4	t_1	t_2	t_4
S1	780	0.8	0.32×10^{-5}	0.64×10^{-5}	1.28×10^{-5}	0.8×10^{-5}	1.6×10^{-5}	3.2×10^{-5}
S2	624	1.0	0.5×10^{-5}	1×10^{-5}	2×10^{-5}	1×10^{-5}	2×10^{-5}	4×10^{-5}
S3	416	1.5	1.125×10^{-5}	2.25×10^{-5}	4.5×10^{-5}	1.5×10^{-5}	3×10^{-5}	6×10^{-5}
S4	312	2.0	2×10^{-5}	4×10^{-5}	8×10^{-5}	2×10^{-5}	4×10^{-5}	8×10^{-5}
S5	208	3.0	0.45×10^{-4}	0.9×10^{-4}	1.8×10^{-4}	0.3×10^{-4}	0.6×10^{-4}	1.2×10^{-4}
S6	156	4.0	0.8×10^{-4}	1.6×10^{-4}	3.2×10^{-4}	0.4×10^{-4}	0.8×10^{-4}	1.6×10^{-4}
S7	104	6.0	1.8×10^{-4}	3.6×10^{-4}	7.2×10^{-4}	0.6×10^{-4}	1.2×10^{-4}	2.4×10^{-4}

Table 3: Typical grid size and number of time steps for the unstructured grids set

Grid	Number of cells in the wedge	$\frac{h_i}{h_1}$	Δt [s]
U1	740	1.000	6.25×10^{-7}
U2	560	1.326	1.11×10^{-6}
U3	383	1.957	2.50×10^{-6}
U4	337	2.230	3.31×10^{-6}
U5	278	2.713	5.00×10^{-6}
U6	205	3.736	1.00×10^{-5}
U7	115	6.866	4.00×10^{-5}

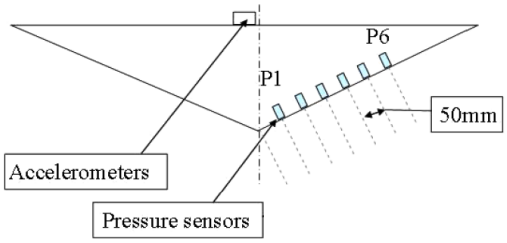

Figure 2: Pressure sensor distribution

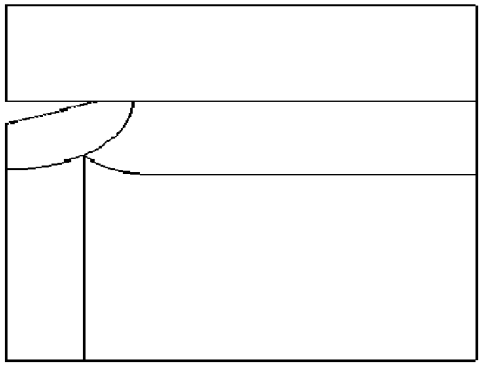

(a) Structured grid

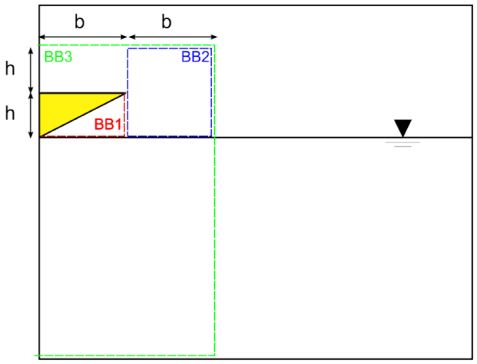

(b) Unstructured grid

Figure 3: Grid topologies

2.4. Quantities of interest

The quantities of interest are: peak pressure in the six sensors; time of peak pressure occurrence in the six sensors; pressure and acceleration at six time instances, integral of the pressure over time for each sensor.

Pressure and acceleration are calculated for six time instances that are defined for fixed and relative times. The time interval used in the calculation of the integrals starts at the time when the maximum pressure for the first sensor occurs and ends 80ms after.

3. Convergence properties of the numerical solution

The calculation of the numerical uncertainties was performed using the in-built tools available at `www.refresco.org`, which are fully described by

Eça and Hoekstra (2009, 2014) and Eça et al. (2010). Therefore, only a summary of the procedure, focusing on the discretization error and assuming that the round-off and iterative errors are neglected, is going to be presented.

For unsteady flow problems the discretization error, ϵ_ϕ, can be based on the Richardson extrapolation:

$$\epsilon_\phi \simeq \delta_{RE} = \phi_i - \phi_0 = \alpha_x h_i^{p_x} + \alpha_t \tau_i^{p_t} \quad (1)$$

where ϕ_i is a local flow quantity, ϕ_0 is the estimate of the exact value, α_x and α_t are constants to be determined, h_i and τ_i are the typical cell and time step sizes, and p_x and p_t are the observed order of convergence for the space and time discretization.

The typical cell size is given by Equation (2) and the typical time size is given by Equation (3).

$$\frac{h_i}{h_1} = \sqrt[N]{\frac{n_1}{n_i}} \quad (2)$$

$$\frac{\tau_i}{\tau_1} = \frac{\Delta t_1}{\Delta t_i} \quad (3)$$

In these equations, the index i refers to a reference typical grid size and time step, n is the number of cells and N is number of dimensions ($N = 1$ or 2 in a two dimensional problem).

These equations can only be employed if the data shows asymptotic monotonic convergence and the data points display no noise. These conditions are only met in the simulation of simple problems. In non-trivial problems, the cause of scatter in the data may derive from several sources, as the lack of geometrical similarity of the grids, the use of too coarse grid sizes or large time steps, and the use of schemes with flux limiters or other types of switches.

In order to deal with the fact that the assumptions required by Equation (1) are rarely met, three other error estimators were introduced. Although these error estimators can be used for both temporal and spatial discretizations, only the ones employed to estimate the error for the spatial discretization are shown.

$$\epsilon_\phi \simeq \delta_1 = \phi_i - \phi_0 = \alpha h_i \quad (4)$$

$$\epsilon_\phi \simeq \delta_2 = \phi_i - \phi_0 = \alpha h_i^2 \quad (5)$$

$$\epsilon_\phi \simeq \delta_{1,2} = \phi_i - \phi_0 = \alpha_1 h_i + \alpha_2 h_i^2 \quad (6)$$

The combination of the above referred spatial and temporal error estimators results in 16 possible ways to estimate the error of an unsteady problem. The applied estimators are chosen based on the values of p_x and p_t. A surface is fitted to the data by minimizing the weighted sum of differences between the error estimator and the data points. The error estimator with smallest standard deviation of the fit, σ, is chosen. To account for the reliability of the various estimates, a safety factor, F_s, is introduced. If the estimated error is considered reliable, then a safety factor equal to 1.25 is used, otherwise, it is set to 3. For the error estimate to be considered reliable, the fit has to be performed using Equation (1), the values of p_x and p_t have to fall in the interval [0.5;2.1] and the value of the standard deviation has to be smaller than the average data range, $\Delta_\phi = (\phi_{max} - \phi_{min})/(N_g - 1)$. Depending on the data noise level, the numerical uncertainty is calculated using Equation (7), if the level of noise is high ($\sigma \geq \Delta_\phi$), or using Equation (8) otherwise.

$$U(\phi_i) = F_s \; min \left(\frac{\sigma}{\Delta_\phi}(\delta + \delta_{fit} + \sigma) \right) \quad (7)$$
$$\phi_{max} - \phi_{min}$$

$$U(\phi_i) = F_s \delta + \delta_{fit} + \sigma \quad (8)$$

with $\delta_{fit} = \phi_i - \phi_{i_{fit}}$, and $\phi_{i_{fit}}$ the value obtained for the fit.

The uncertainty was estimated for three sets of simulations. One using unstructured grids and first order implicit Euler (Table 3), and the others using structured grids with both time schemes (Table 2).

Initial conditions impose an error, since there is an air flow acting on the wedge that is dependent on the grid and time step refinement. In order to reduce the impact of this error in the calculation of accelerations and pressures at absolute time instances, two methods were used:

- fixed times, i.e., the same times for all grids and time steps;
- relative times referred to the time when the maximum pressure in sensor 1 occurs.

It was observed that the use of relative times allowed to obtain a smaller uncertainty in 51.4% of the cases for the accelerations and 68.1% for the pressures, so they were used in the validation process.

The convergence properties of local (maximum pressure) and functional (pressure integral) quantities were also compared. This comparison lead to conclude that they were affected in opposite ways by the pressure rise time: the sharper it is, the greater is the uncertainty for the maximum pressure and smaller for the pressure integral.

4. Sensitivity studies

In this section the results obtained for the sensitivity studies of the temporal discretization scheme, domain size and the grid type are presented.

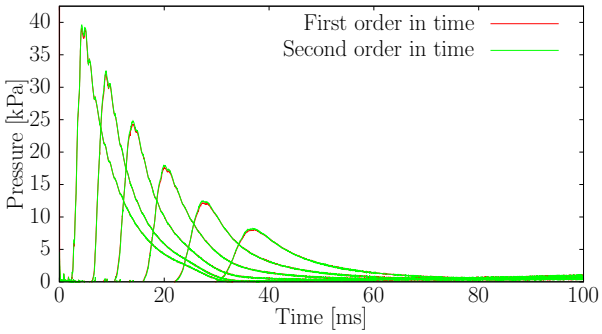

(a) Pressure, unstructured grid U6 with 10000 time steps

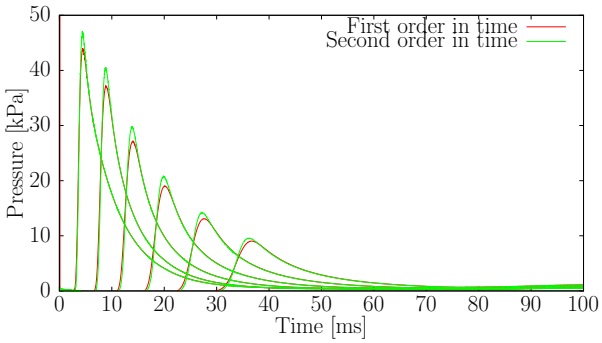

(b) Pressure, structured grid S4 with 5000 time steps

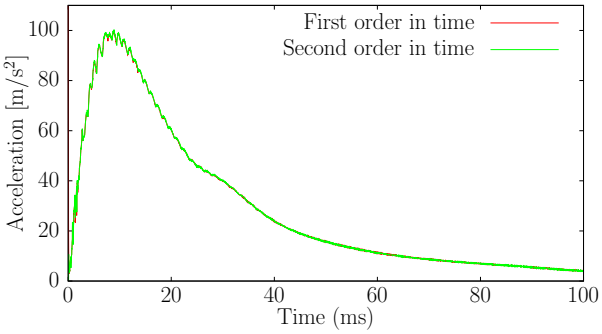

(c) Acceleration, unstructured grid U6 with 10000 time steps

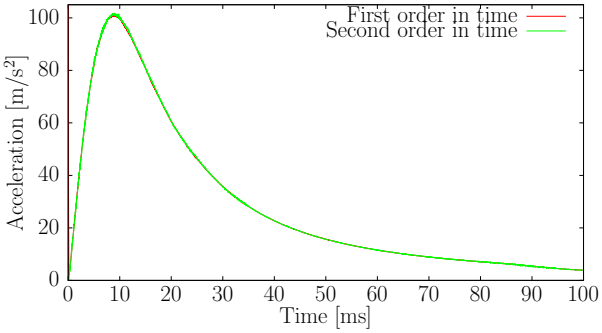

(d) Acceleration, structured grid S4 with 5000 time steps

Figure 4: Evolution of pressure and acceleration for simulation performed using unstructured and structured grids with different time derivative approximations

4.1. Temporal scheme

The comparison of the results obtained using both temporal schemes available in ReFRESCO are presented in Figure 4. The results show that for the case of the unstructured grid the differences are smaller than in the case of the structured grids. This is related to the fact that the time step used in the unstructured grid simulation is much smaller than the ones used for the structured grids. Looking only at the results obtained using the structured grids, it is possible to conclude that the use of the second order three time level scheme allows to obtain sharper pressure rises and greater peak pressure values using larger time steps. This leads to smaller uncertainties for the peak pressures. The effect of the time derivative approximation in the acceleration behaviour is small for both grid types: for the maximum acceleration it is around 0.2% in the unstructured grid and approximately 1% in the structured one.

Concerning the numerical uncertainty value, none of the derivative approximations has the upper hand, so the comparison was made considering the obtained maximum and minimum values of uncertainty. Both the maximum and minimal numerical uncertainties are smaller when using the 2nd time derivative approximation.

4.2. Domain size influence

The influence of the domain size was investigated for both grid types, but only the results for the structured grid are presented.

Figure 5 shows two examples of the influence that different domain dimensions have in the numerical results. Three features are clear:

- Reducing the domain dimensions have a significant impact in the results;
- The numerical results are more sensitive to variations of water depth, WD;
- The proportional variation is a combination of the variations of the three independent dimensions.

Based on the results obtained by proportionally changing the domain dimensions an input uncertainty, U_{input}, was calculated, using the previously described method.

4.3. Grid type

The pressure and acceleration evolutions in Figure 4 display non physical oscillations in the results obtained using the unstructured grids that do not occur in the structured grid calculations. To evaluate if this behaviour was related to the grid type and not to existing differences in the convergence criteria of the different equations two unstructured grids (U1 and U6), were simulated using the same settings as the structured grids S1 (8000 time steps) and S5 (640 time steps) with first order in the time derivative approximation.

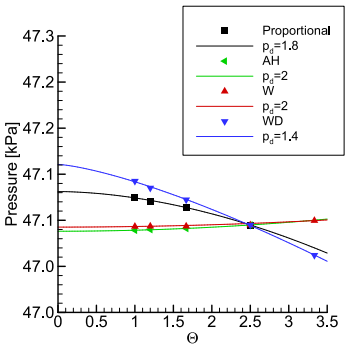

(a) Maximum Pressure in sensor 1

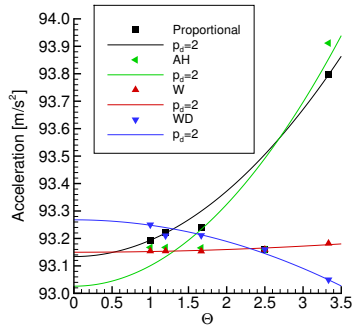

(b) Acceleration for relative time 1

Figure 5: Comparison between the results obtained with structured and unstructured grids

The results are presented in Figure 6, and show that the existing oscillations are related to the grid type. It is also important to refer that when performing this simulations the convergence criteria was not met for several time steps when using the unstructured grids.

Both Figures 4 and 6 show that the evolution of pressure is similar in both grids, but in relation to acceleration there are significant differences in the interval from 25 to 40ms. For the finest grids and smallest time steps the differences between peak pressures are less than 4.5%.

Although the numerical uncertainty is not always greater when using unstructured grids, the maximum uncertainty for the unstructured grid calculations is significantly higher: 15.35kPa in the unstructured grid and 7.59kPa in the structured.

5. Validation

The main objective of this work is to assess the modelling error of the mathematical model. For this purpose, the validation procedure proposed in ASME (2009), that aims at estimating the modelling error, δ_{model}, is followed.

The errors affecting the numerical results, S, are: the modelling error, δ_{model}; the numerical error, δ_{ϕ}; and the input error, δ_{input}. The experimental results, D, are affected by the experimental error, δ_{exp}. Therefore the validation

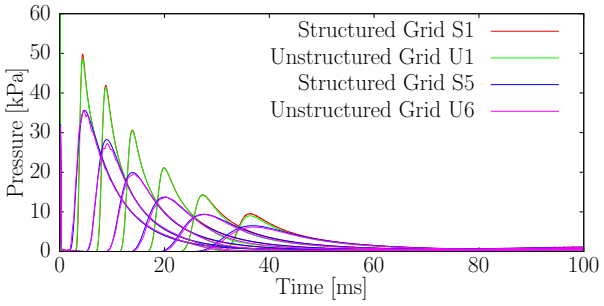

(a) Pressure

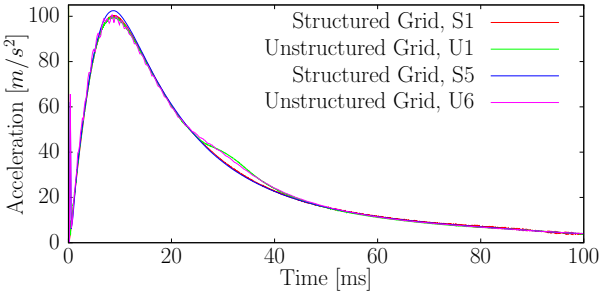

(b) Acceleration

Figure 6: Comparison of the evolution of pressure and acceleration between structured and unstructured grids

comparison error, E, can be defined as:

$$E = S - D = \delta_{model} + (\delta_{\phi} + \delta_{input} - \delta_D) \quad (9)$$

Although the value of E is known, the magnitudes and signs of δ_{ϕ}, δ_{input} and δ_D have to be estimated. This estimate is called validation uncertainty, U_{val}, and it is calculated from Equation 10.

$$U_{val} = \sqrt{U_{\phi}^2 + U_{input}^2 + U_{exp}^2} \quad (10)$$

where U_{ϕ} is the numerical uncertainty, U_{exp} is the experimental uncertainty, U_{input} is the input uncertainty. In this case, the latter is assumed to be the uncertainty due to the domain size, U_{domain}.

Taking into account the relation presented in Equation (9) and the definition of U_{val}, it is possible to conclude, with a 95% confidence level, that the modelling error falls in the following interval:

$$\delta_{model} \in [E - U_{val}; E + U_{val}] \quad (11)$$

The experimental results used in this validation exercise were obtained by Lewis et al. (2010). Moreover, the results an analysis of the experimental uncertainties was also made by the same authors.

The quantities of interest that are going to be compared are the pressure and acceleration at six time instances, the maximum pressure, and decaying time, i.e., the time difference between the maximum pressure in a given sensor and in sensor 1.

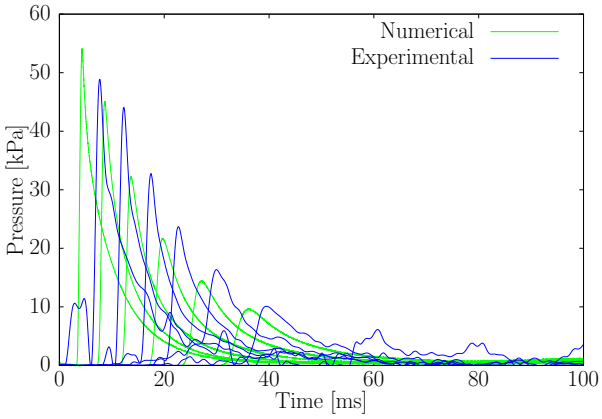

(a) Pressure evolution

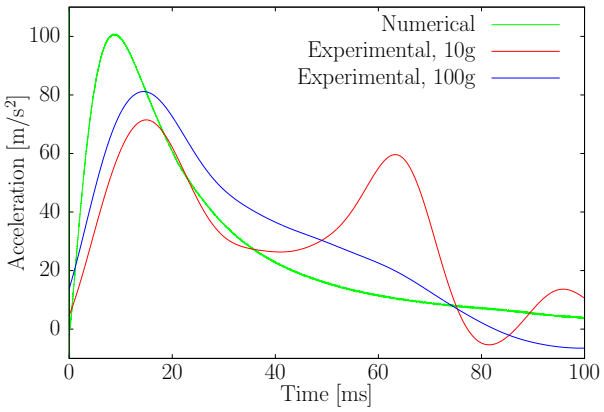

(b) Comparison between the numerical and experimental results for the evolution of acceleration

Figure 7: Comparison between the numerical and experimental values of the acceleration and pressure evolutions

Table 4: Comparison between the numerical (S) and experimental (D) values

Maximum pressure [kPa]							
Sensor	S	D	E	U_{num}	U_{input}	U_{exp}	U_{val}
1	54.14	48.91	5.24	6.19	0.05	3.81	7.26
2	45.11	44.05	1.06	1.05	0.08	3.81	3.95
3	32.19	32.78	-0.59	1.48	0.15	3.81	4.09
4	21.62	23.70	-2.08	1.62	0.03	3.81	4.13
5	14.40	16.35	-1.95	0.67	0.06	3.81	3.86
6	9.61	10.09	-0.49	0.11	0.03	3.81	3.81
Pressure at relative times [kPa]							
Time	S	D	E	U_{num}	U_{input}	U_{exp}	U_{val}
1	31.53	29.25	2.29	0.08	0.10	3.81	3.81
2	25.15	24.57	0.58	0.08	0.04	3.81	3.81
3	19.33	19.76	-0.43	0.10	0.11	3.81	3.81
4	14.96	14.15	0.81	0.11	0.01	3.81	3.81
5	11.33	11.11	0.23	0.18	0.07	3.81	3.81
6	7.70	8.02	-0.32	0.35	0.08	3.81	3.82
Time difference between the maximum pressure in a given sensor and in sensor 1 [ms]							
Sensor	S	D	E	U_{num}	U_{input}	U_{exp}	U_{val}
2	4.31	4.60	-0.29	0.13	0.004	0.50	0.52
3	9.32	9.77	-0.45	0.06	0.03	0.50	0.50
4	15.37	15.01	0.37	0.42	0.03	0.50	0.65
5	22.75	22.27	0.48	0.14	0.57	0.50	0.77
6	31.81	31.79	0.03	0.56	0.06	0.50	0.75

Acceleration [m/s^2]											
Time	S	D		E		U_{num}	U_{input}	U_{exp}		U_{val}	
		10g	100g	10g	100g			10g	100g	10g	100g
1	93.98	59.94	72.92	34.04	21.05	1.88	0.29	1.08	11.77	2.19	11.92
2	96.93	71.30	81.15	25.63	15.78	3.81	0.34	1.08	11.77	3.98	12.38
3	75.84	63.69	73.89	12.15	1.95	0.90	0.40	1.08	11.77	1.47	11.81
4	53.56	42.13	56.96	11.43	-3.40	0.41	0.33	1.08	11.77	1.20	11.78
5	36.72	28.62	43.60	8.09	-6.88	0.84	0.33	1.08	11.77	1.41	11.81
6	23.60	26.48	34.60	-2.88	-11.01	0.11	0.55	1.08	11.77	1.22	11.79

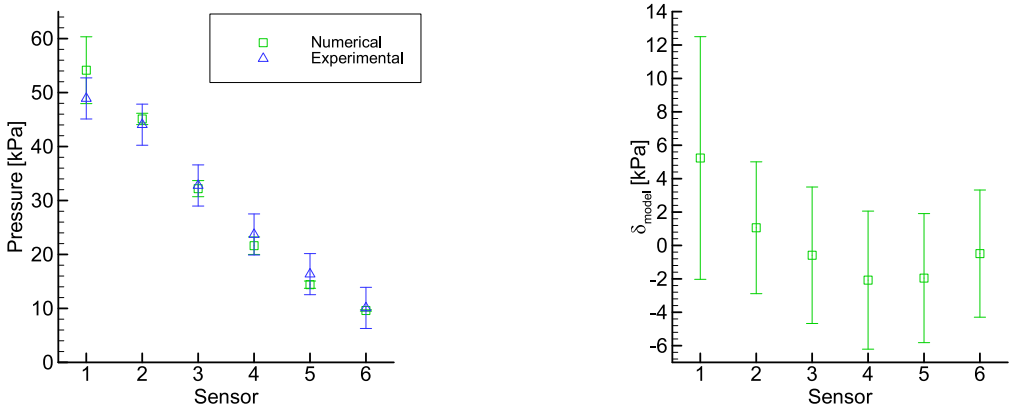

(a) Maximum pressure

(b) Modelling error, δ_{model}

Figure 8: Comparison between the numerical and experimental values of the maximum pressure at the sensors and the associated modelling error

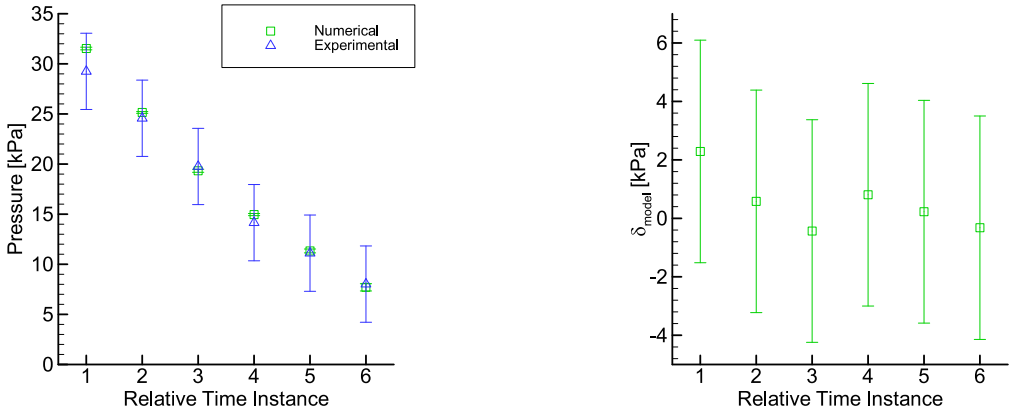

(a) Pressure at relative time instances

(b) Modelling error, δ_{model}

Figure 9: Comparison between the numerical and experimental values of the pressure at different relative time instances and the associated modelling error

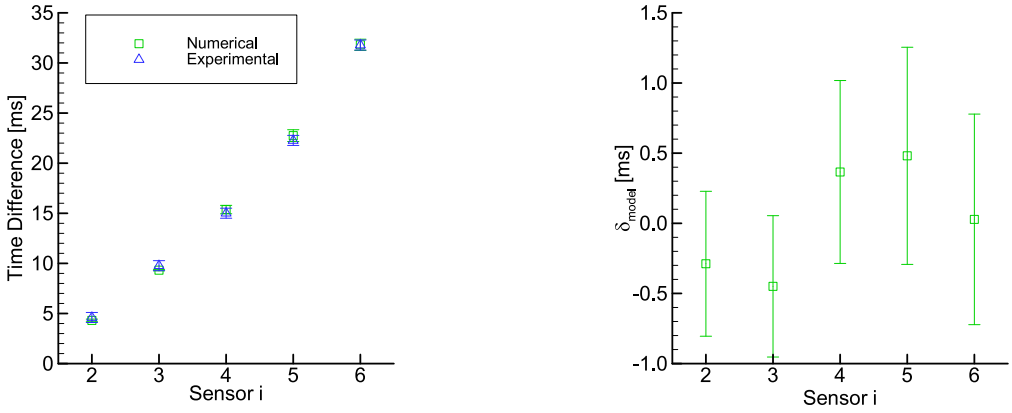

(a) Decaying time

(b) Modelling error, δ_{model}

Figure 10: Comparison between the numerical and experimental values of the difference between the time of peak pressure occurrence in sensor i and the same time for sensor 1

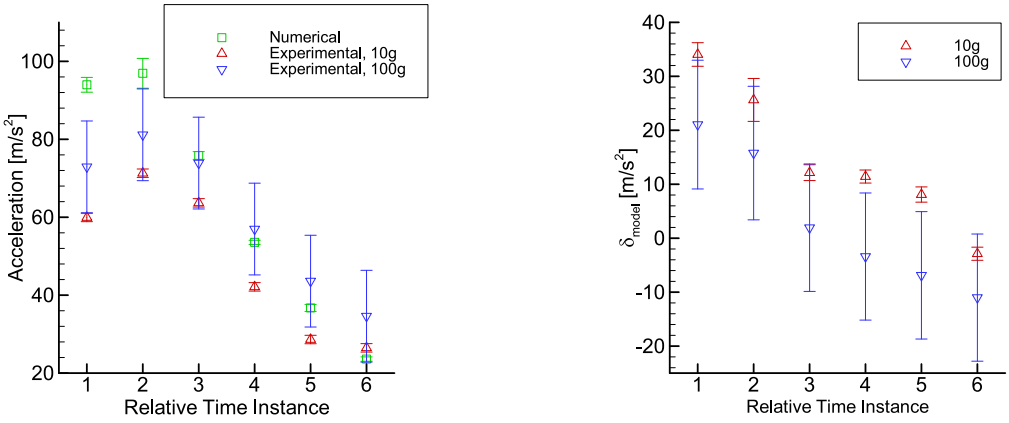

(a) Acceleration at relative time instances

(b) Modelling error, δ_{model}

Figure 11: Comparison between the numerical and experimental values of the acceleration at different time instances and the associated modelling error

Figure 7 shows the comparison between the numerical and experimental results for the evolution of acceleration and pressure. The numerical and experimental values, the validation comparison error, the uncertainties involved in the calculation of U_{val} and its value for the different quantities referred above are presented in Table 4.

Figures 8 through 11 enable a visualization of the data presented in Table 4.

Although Figure 7a shows a delay between the pressure experimental results and the numerical, the maximum pressure values and the pressure for relative time instances agree quite well with the experimental results. For these quantities of interest the modelling error, δ_{model}, is between -6kPa and 6kPa, except in the maximum pressure in sensor 1 where it reachs 12.5kPa (Figures 8 and 9). Concerning the time difference between peak pressures, the δ_{model} value is estimated to be between -0.95ms and 1.25ms (Figure 10). Table 4 also shows that U_{val} values for these quantities are clearly dominated by the experimental uncertainty. In most cases the experimental uncertainty, U_{exp}, accounts for more than 85% of the validation uncertainty. Only in the case of the maximum pressure in sensor 1, where the experimental uncertainty is smaller than the numerical uncertainty, corresponding to 27.4% of U_{val}. This values suggest that to reduce the modelling error interval focus should be given to improving the experimental set-up.

Acceleration evolution show considerable differences between the numerical and experimental results depicted in Figures 7b and 7b and Table 4. Figure 7b shows that the maximum δ_{model} value is approximately 36m/s^2, which is approximately 36% of the maximum acceleration value obtained in the numerical simulations. A reason for the large δ_{model} values may be the fact that the used mathematical model does not account for the effect of the tank floor, as it considers the water depth, WD, to be 2.1m, this value is quite different from the experimental set-up, where WD is only 0.59m. Despite this variation in WD, the differences in the experimental results obtained for both accelerometers and the existence of non-physical behaviours, such as inflexions points and two maxima in the case of the 10g accelerometer, suggest that the experimental results are not reliable.

6. Conclusions

In the present work a validation exercise of the numerical code ReFRESCO for the impact of a bidimensional wedge with 25° deadrise angle based on the experimental results of Lewis et al. (2010) is presented.

The use of relative times allows to reduce the influence of the error imposed by the initial condition. The convergence behaviour of local (maximum pressure) and functional (pressure integral) quantities are affected in opposite ways by the pressure rise time. As expected, it was also noted that the choice of point combinations in the numerical uncertainty has a great influence in the estimated value.

Regarding the sensitivity studies, the use of a second order three time level scheme is advised since it allows to obtain smaller uncertainty values using larger time step sizes. However, some robustness issues were encountered using this derivative approximation when performing the domain sensitivity study for the unstructured grids. In relation to the influence of the domain dimensions in the numerical results, it can be concluded that the water depth, WD, is the most influential dimension and that the domain dimensions initially chosen were correct, since a small input error was obtained for all quantities. As expected, structured grids produced better

quality results, from which smaller numerical uncertainties were obtained. When using structured grids the numerical solution did not present the non physical oscillations exhibited when unstructured grids were used.

Though a time difference between the numerical and experimental results for both pressure and acceleration was detected, the numerical peak pressure values for each sensor and pressure values for relative times presented a good agreement with the experimental results. It was also possible to verify that the same occurred for the time difference between the peak pressures for one sensor and for the first. For these quantities of interest the U_{val} values suggest that improvements to experimental program should be performed.

Despite the good results obtained for pressure related quantities, experimental and numerical acceleration values show great differences, suggesting that the experimental acceleration data was not reliable.

Acknowledgements

The author would like to acknowledge the guidance and support of Professor Luís Eça and António Maximiano. Special thanks are due to WavEC-Offshore Renewables for providing the computational resources required for the numerical simulations.

References

ASME (2009), *Standard for Verification and Validation in Computational Fluid Dynamics and Heat Transfer: ASME V&V 20-2009*, American Society of Mechanical Engineers.

Eça, L. (2003), Grid generation tools for structured grids, Technical report, Instituto Superior Técnico.

Eça, L. and Hoekstra, M. (2009), 'Evaluation of numerical error estimation based on grid refinement studies with the method of the manufactured solutions', *Computers & Fluids* **38**(8), 1580–1591.

Eça, L. and Hoekstra, M. (2014), 'A procedure for the estimation of the numerical uncertainty of cfd calculations based on grid refinement studies', *Journal of Computational Physics* **262**, 104 – 130.

Eça, L., Vaz, G. and Hoekstra, M. (2010), A verification and validation exercise for the flow over a backward step, *in* 'V European Conference on Computational Fluid Dynamics'.

Ellis, S. (2015), 'Engineers prepare for orion water-impact testing with precision to protect future astronauts', `https://www.nasa.gov/feature/langley/engineers-prepare-for-orion-water-impact-testing-with-precision-to-protect-future-astronauts`. Acessed: 18/08/2017.

Hirt, C. and Nichols, B. (1981), 'Volume of fluid (VOF) method for the dynamics of free boundaries', *Journal of Computacional Physics* **39**, 201–225.

Kamath, A., Bihs, H. and Arntsen, Ø. A. (2016), Study of water impact and entry of a free falling wedge using cfd simulations, *in* '35^{th} Internacional Conference on Ocean, Offshore and Artic Engineering'.

Lewis, S. G., Hudson, D. A., Turnock, S. R. and Taunton, D. J. (2010), 'Impact of a free-falling wedge with water: synchronized visualization, pressure and acceleration measurements', *Fluid Dynamics Research* **42**(3), 035509.

MARIN (2017), 'ReFRESCO', `http://www.marin.nl/web/Facilities-Tools/CFD/ReFRESCO.htm`. Acessed:10/08/2017.

Maximiano, A. (2016), CFD verification and validation of a 2d wedge entry in otherwise calm water, Technical report, MARIN.

Qian, L., Causon, D., Mingham, C. and Ingram, D. (2006), 'A free-surface capturing method for two fluid flows with moving bodies', *Proceedings of the Royal Society of London A: Mathematical, Physical and Engineering Sciences* **462**(2065), 21–42.

Reddy, D., Scanlon, T. and Kuo, C. (2002), Prediction of slam loads on wedge section using computacional fluid dynamics (CFD) techniques, *in* '24^{th} Symposium on Naval Hydrodynamics Fukuoka, Japan'.

Sasson, M., Chai, S., Beck, G., Jin, Y. and Rafieshahraki, J. (2016), 'A comparison between smoothed-particle hydrodynamics and RANS volume of fluid method in modelling slamming', *Journal of Ocena and Science* **1**, 119–128.

von Karman, T. (1929), 'The impact on seaplane floats during landing', *NACA Thecnical Note n^o 321* .

Wagner, H. (1932), 'Über stoß- und gleitvorgänge an der oberfläche von flüssigkeiten', *ZAMM - Journal of Applied Mathematics and Mechanics / Zeitschrift für Angewandte Mathematik und Mechanik* **12**(4), 193–215.

Wang, J., Lugni, C. and Faltinsen, O. M. (2015), 'Experimental and numerical investigation of a freefall wedge vertically entering the water surface', *Applied Ocean Research* **51**, 181–203.